Chemistry–A European Journal
Research Article
doi.org/10.1002/chem.202404672
Chemistry Europe
European Chemical Societies Publishing
www.chemeurj.org

Should I stay or should I flow? An exploration of phase-separated metallosupramolecular liquid crystal polymers

Charlie A. Lindberg,[a] Alice E. Roberson,[b] Elina Ghimire,[a] Jerald E. Hertzog,[a] Nicholas R. Boynton,[a] Guancen Liu,[b] Deborah K. Schneiderman,[a] Shrayesh N. Patel,[a] and Stuart J. Rowan*[a, b, c]

Dynamic liquid crystalline polymers (dLCPs) incorporate both liquid crystalline mesogens and dynamic bonds into a single polymeric material. These dual functionalities impart order-dependent thermo-responsive mechano-optical properties and enhanced reprocessability/programmability enabling their use as soft actuators, adaptive adhesives, and damping materials. While many previous works studying dynamic LCPs utilize dynamic covalent bonds, metallosupramolecular bonds provide a modular platform where a series of materials can be accessed from a single polymeric feedstock through the variation of the metal ion used. A series of dLCPs were prepared by the addition of metal salts to a telechelic 2,6-bisbenzimidazolylpyridine (Bip) ligand endcapped LCP to form metallosupramolecular liquid crystal polymers (MSLCPs). The resulting MSLCPs were found to phase separate into hard and soft phases which aids in their mechanical robustness. Variations of the metal salts used to access these materials allowed for control of the thermomechanical, viscoelastic, and adhesive properties with relaxations that can be tailored independently of the mesogenic transition. This work demonstrates that by accessing phase separation through the incorporation of metallosupramolecular moieties, highly processable yet robust MSLCP materials can be realized. This class of materials opens the door to LCPs with bulk flow behavior that can also be utilized as multi-level adhesives.

1. Introduction

Liquid crystal polymers (LCPs) are a class of materials characterized by the covalent incorporation of liquid crystalline moieties (mesogens) into a polymeric structure.[1,2] LCP materials include traditional linear polymeric species as well as crosslinked systems such as liquid crystal networks (LCNs) and liquid crystal elastomers (LCEs).[3–5] By selectively manipulating the orientation of these mesogens and/or disrupting the liquid crystalline phase via an external stimulus (e.g., heat or light), it is possible to induce functional responses in these materials such as complex optical transformations,[6–8] thermally-induced shape memory,[9–11] and "soft elastic" damping behavior stemming from the mesogens' rotational modes.[12–14] Due to the interplay between the entropic elasticity afforded by the network structure and the reversible assembly of the liquid crystal (LC) domain structure, crosslinked LCPs have been studied for use in a wide array of application spaces including reversible actuators,[15,16] biomedical devices,[17,18] and adaptive adhesives.[19–21]

One drawback of many permanently crosslinked polymer networks is the inability to undergo further reprocessing once crosslinking has occurred, making reprogramming and reprocessing efforts futile. One avenue to circumvent this shortcoming has been the incorporation of dynamic covalent chemistries into the network structure as a means of providing linkages that can reversibly cleave to induce structural reorganization.[22–24] Dynamically crosslinked LCP materials have also been studied in this regard, demonstrating that the incorporation of dynamic bonds can facilitate both reprocessability as well as post-synthetic programmability.[25–27] However, while reprocessability is achievable for many of these systems, it often requires rather harsh processing conditions[28–31] due to the inherent tradeoff between stability and processability in dynamic polymer systems and the need to balance the two.[32,33]

One potential route to enhance the processability of dynamic materials is the use of more labile linkages to facilitate network exchange under more moderate conditions. An obvious drawback to this approach is the diminishing stability that comes with the incorporation of a more labile dynamic linkage. However, there are a number of examples of dynamic polymer systems

[a] C. A. Lindberg, E. Ghimire, J. E. Hertzog, N. R. Boynton, D. K. Schneiderman, S. N. Patel, S. J. Rowan
Pritzker School of Molecular Engineering, The University of Chicago, Chicago, Illinois, USA
E-mail: stuartrowan@uchicago.edu
[b] A. E. Roberson, G. Liu, S. J. Rowan
Department of Chemistry, The University of Chicago, Chicago, Illinois, USA
[c] S. J. Rowan
Chemical Science and Engineering Division and Center for Molecular Engineering, Argonne National Laboratory, Lemont, Illinois, USA

Supporting information for this article is available on the WWW under https://doi.org/10.1002/chem.202404672

that utilize weak dynamic bonds in combination with phase separation[34–37] to yield robust materials.[38–41] Supramolecular polymers formed from (macro)monomers polymerized through noncovalent interactions, such as ionic bonds, hydrogen bonding, or host-guest interactions, are a class of dynamic polymers that have been used to access robust functional materials.[42–47] A subclass of supramolecular polymers are the metallosupramolecular polymers (MSPs), in which metal-ligand coordination is the driving force to form the polymers.[48–54] MSPs are particularly interesting as there is a wide range of accessible bond strengths and connectivities based on different metal ion/ligand pairs.[55–62] Metallosupramolecular interactions have been previously incorporated into crosslinked LCP materials as a modality for introducing new adaptive/functional properties such as chemo-based actuation,[63] shape fixing,[64] and programmability.[65] However, little work has been conducted on the utilization of metallosupramolecular interactions as the driving force to form LCPs from lower molecular weight (macro)monomers. Work by Liang et al.[66] took inspiration from the protein chemistry of mussels and created catechol-terminated liquid crystalline polymers which were crosslinked with an Fe (III) salt. The use of these strong metallosupramolecular linkages resulted in materials that formed tough, processable films capable of shape-memory behavior. That work showed that metal-ligand linkages could be successfully incorporated into LCPs without significantly disrupting the LC phase. Work reported herein focuses on the design, synthesis, and characterization of metallosupramolecular liquid crystal polymers (MSLCPs) with the goal of exploring how altering the nature of the metal-ligand interactions can be used to impact the thermomechanical, viscoelastic, and adhesive properties of these materials. More specifically, the target telechelic LCP macromonomers will bear terminal bis(benzimidazolyl)pyridine (Bip) ligands (Figure 1A). It has previously been shown that the Bip ligand is capable of binding to a variety of metal ions and has been studied extensively in the context of MSPs.[39,58,67–71] Importantly for this study it has been shown that Bip can bind to Zn(II) ions in a 2:1 ratio and to lanthanides, such as Eu(III), in a 3:1 ratio (Figure 1B, Figures S1–S3).[69]

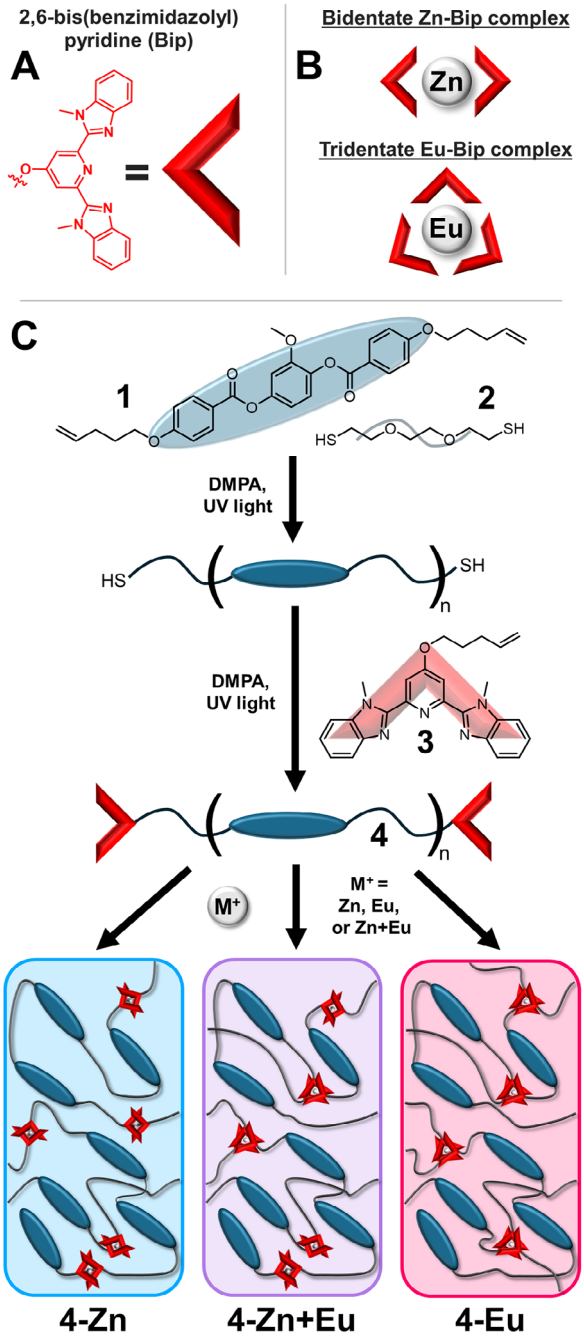

Figure 1. (A) Chemical structure of the 2,6-bis(benzimidazolyl)-pyridine ligand; (B) Diagrams of the different connectivities that the Bip ligand can adopt depending on the metal ion (Zn(II) or Eu(III)); (C) Component and polymeric architectures for a modular MSLCP material that allows for selective metallosupramolecular connectivities based on the metal adding where Zn(II) provides linear linkages, Eu(III) provides crosslinks, and a mixture of Zn(II) and Eu(III) provides both.

2. Results and Discussion

A dialkene mesogenic monomer (**1**) was reacted with a dithiol chain extender (**2**) and an alkene-bearing Bip ligand (**3**) using photoinitiated thiol-ene chemistry to synthesize the telechelate LCP (**4**) (Figure 1C). Using the Carothers equation, the ratio of **1** and **2** was calculated to target a polymer with a molecular weight of around 10,000 g/mol with thiol end groups. The monomers were dissolved in methylene chloride (DCM) with a catalytic amount of the photoinitiator 2,2-dimethoxy-2-phenylacetophenone (DMPA). The reaction solution was then exposed to UV light (320–390 nm, 3 mW cm^{-2}) for 15 min to initiate the polymerization. Full conversion of the alkene moieties was confirmed via ^{1}H-NMR spectroscopy via the disappearance of the signal corresponding to the alkene protons (Figure S4). A stoichiometric amount of **3** (relative to thiol chain ends of the polymer) and a catalytic amount of DMPA were then added to the reaction solution, which was then irradiated by UV light to initiate this thiol-ene coupling of the ligand to the polymer chain ends. As before, full conversion was confirmed by the disappearance of the alkene protons signals in the ^{1}H-NMR (Figure S4). The telechelate polymers (**4**) were then purified via precipitation in methanol (MeOH). ^{1}H-NMR of the purified polymer

confirmed a number-average molecular weight (M_n) of approximately 10,000 g mol^{-1}, as calculated by comparing the chain end and mesogenic proton signals (Figure S5). Gel permeation chromatography (GPC) versus polystyrene standards further verified the molecular weight of the LCPs with an M_n of 8500 g mol^{-1} and a $Đ$ of 1.3 (Figure S6). To access the desired MSLCPs, **4** was mixed with the metal salts zinc di[bis(trifluoromethylsulfonyl)imide] ($Zn(NTf_2)_2$) and europium tri[bis(trifluoromethylsulfonyl)imide] ($Eu(NTf_2)_3$).[69] These metal ions not only bind in different stoichiometries with the Bip ligand but also exhibit significantly different binding strengths–the formed Zn:Bip complex (~10^6 M^{-2}) and Eu:Bip complex (~10^3-10^4 M^{-3}).[49,72,73] To form the MSLCPs, **4** was dissolved in chloroform ($CHCl_3$) with a stoichiometric amount (such that each Zn(II) ion would complex to two Bip ligands and each Eu(III) ion would complex to three Bip ligands) of $Zn(NTf_2)_2$ (**4-Zn**), $Eu(NTf_2)_3$ (**4-Eu**), or a 50/50 mixture of $Zn(NTf_2)_2$ and $Eu(NTf_2)_3$ (**4-Zn+Eu**). The resulting solutions were cast into films and dried under vacuum (16 h, 60°C) to remove any residual solvent. The films were then melt processed (5 min, 130°C, 4 tons) to form homogeneous films for testing (Figure S7A). As a confirmation of the formation of stable metal-ligand complexes in the bulk material, the films were imaged under UV light (Figure S7B). The color of the observed fluorescence directly corresponds to the nature of the complex formed with the Zn:Bip complex fluorescing blue, the Eu:Bip complex fluorescing red, and the mixed system fluorescing purple as a combination of the two. Thermogravimetric analysis (TGA) was performed on the materials to determine the materials' thermal stability with all materials exhibiting a primary degradation onset temperature between 325°C and 335°C (Figure S8) which is well above any temperature accessed for any further characterization in this work.

The thermal transitions of the prepared MSLCPs were then studied using differential scanning calorimetry (DSC). The DSC thermograms revealed the existence of two transitions in the parent telechelate polymer **4** and three transitions for each of the MSLCPs (Figure 2A). Each material exhibits a glass transition temperature (T_g) below room temperature with **4**, **4-Zn**, **4-Zn+Eu**, and **4-Eu** possessing T_g's of 2°C, 4°C, 8°C, and 4°C, respectively (measured by the midpoint of the step present in the DSC thermogram). Every material also displays an endotherm peak indicative of the clearing temperature (T_C) inherent to the liquid crystalline domains formed in the material where **4**, **4-Zn**, **4-Zn+Eu**, and **4-Eu** have T_C's of 66°C, 81°C, 76°C, and 72°C, respectively. In addition, the width of the T_C appears to broaden as the amount of Eu(III) in the material increases with **4-Zn** having the narrowest T_C and **4-Eu** having the broadest, which follows the literature precedent of more crosslinked LCPs displaying broader T_C's.[74] As mentioned above, the MSLCP materials exhibit an additional higher temperature third transition consistent with what has been seen previously in MSPs.[58,68,75,76] This third transition which is not present in the parent telechelate polymer is assigned as an upper transition (T_{UT}) potentially corresponding to a hard phase formed in the material. **4-Zn**, **4-Zn+Eu**, and **4-Eu** displayed T_{UT}'s of 126°C, 128°C, and 128°C, respectively. Interestingly, this transition consists of two peaks (Figure S9) that shift to slightly higher temperatures and decrease in intensity when

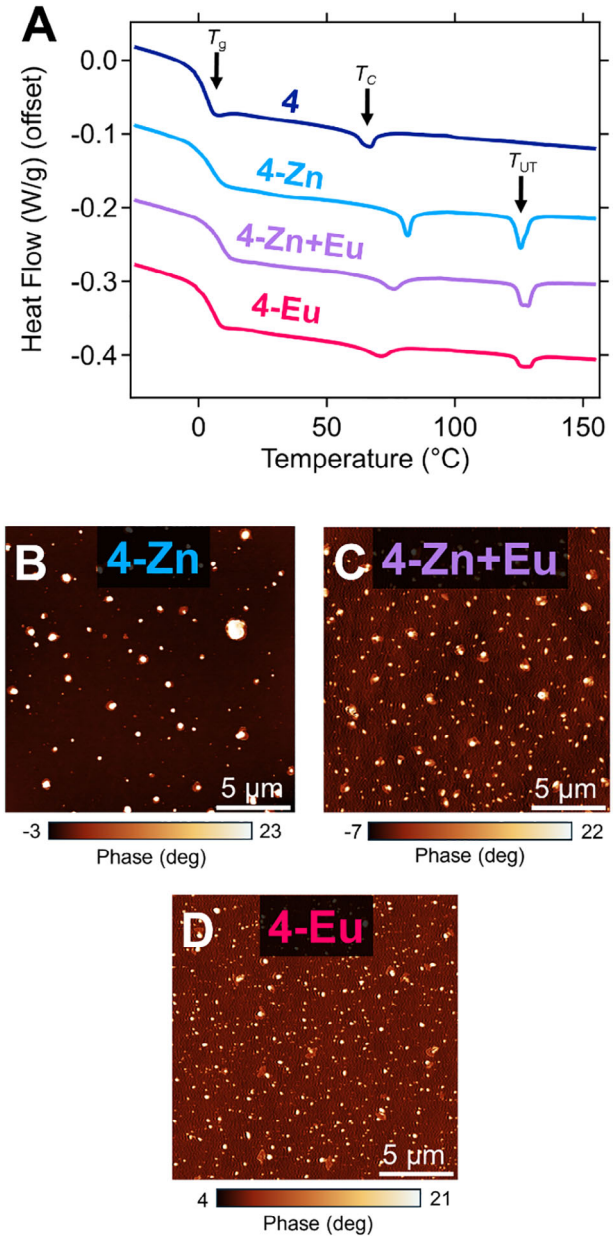

Figure 2. (A) Differential scanning calorimetry thermograms of MSLCP materials; (B) A representative atomic force microscopy phase image of **4-Zn**; (C) A representative atomic force microscopy phase image of **4-Zn+Eu** (D) A representative atomic force microscopy phase image of **4-Eu**.

replacing the Zn(II) ions with the Eu(III) ions. Variable temperature polarized optical microscopy (POM) was also performed to determine the liquid crystalline character of the metallated samples at different temperatures relative to the endotherms observed in DSC (Figure S10A–C). All metallated samples exhibit a birefringent liquid crystalline phase at temperatures below their respective T_C's that clears to an isotropic state above T_C, as evidenced by the disappearance of the birefringence. No further changes to the images are observed at higher temperatures on either side of the T_{UT} suggesting that any change corresponding to the upper endotherm is occurring at length scales not observable by optical microscopy. To confirm the presence

of a phase-separated structure in the MSLCP materials as suggested by the DSC thermograms, atomic force microscopy (AFM) was employed to ascertain the morphology of the materials. AFM measurements were performed on cast samples of **4**, **4-Zn**, **4-Zn+Eu**, and **4-Eu** at 25°C (above the glass transition for all materials). While the AFM height images do not show a large contrast indicative of features in **4-Zn** (Figure S11A), smaller features can be made out in the case of **4-Zn+Eu** and **4-Eu** (Figure S11B–C). The phase images for the metallated materials on the other hand clearly illustrate the presence of a hard and soft phase in each of the materials with larger hard phases in **4-Zn** (Figure 2B), smaller hard phases in **4-Eu** (Figure 2C), and a mixture of the two sizes in **4-Zn+Eu** (Figure 2D) while the phase image of **4** (Figure S12) shows no features. To determine the impact of metal-ligand stoichiometry on the formation of the phase-separated architecture, two additional off-stoichiometry materials were synthesized, **4-Zn$_{80}$** and **4-Zn$_{95}$**, which possessed ratios of Zn(II) ion to ditopic macromonomer of 0.8:1 and 0.95:1, respectively. DSC thermograms (Figure S13A) show the absence of T_{UT}'s in both **4-Zn$_{80}$** and **4-Zn$_{95}$** suggesting that stoichiometry is important in the formation of hard phase that exhibits a bulk endotherm. Interestingly, AFM images taken of films of these materials (Figure S13B–D) reveal that while **4-Zn$_{80}$** lacks a phase-separated structure, **4-Zn$_{95}$** does appear to exhibit some phase-separation albeit not to the extent that is present in **4-Zn**, as evidenced by the lower contrast between the phases in the **4-Zn$_{95}$** image. Both the DSC and AFM data imply a dependence on stoichiometry in the formation of robust hard phases in MSLCP materials. Temperature-dependent wide-angle x-ray scattering (WAXS) experiments were performed across a range of temperatures to elucidate any ordering at smaller length scales. Room temperature measurements of each of the MSLCP materials displayed two signals in the WAXS regime (Figure 3A), a signal at a q-value of 1.4 Å^{-1} (d = 0.4 nm) corresponding to an amorphous polymer scattering distance between mesogens on neighboring polymer chains and a signal at a q-value of 0.16 Å^{-1} (d = 3.8 nm) that is consistent with the mesogen-to-mesogen distance along the backbone of the same polymer chain. The strength of the room temperature signal at q = 0.16 Å^{-1} decreases with an increase in Eu(III) content which falls in line with the subsequent decrease in locally aligned character of the samples possibly as a result of the formation of branching points. A series of temperature sweeps were also performed to determine the thermoreversibility of the structures present in the materials. From room temperature (22°C), the samples were heated to 50°C, 100°C, and 150°C and cooled back through those same temperatures to relate any structural changes to the thermal transitions observed in DSC. In all the materials the signal at q = 1.4 Å^{-1} showed no significant change in peak shape or location at any of the temperatures tested. For **4-Zn** and **4-Zn+Eu** (Figure 3B, Figure S14), the peak at q = 0.16 Å^{-1} decreases in intensity at 50°C and disappears by 100°C. This coincides with the DSC peak assigned to the T_C suggesting the WAXS peak at q = 0.16 Å^{-1} is related to the liquid crystalline ordering of the material. Upon equilibration at 50°C during cooling, this peak reappears in both samples, demonstrating the reversibility of the mesogenic ordering with temperature. For **4-Eu**, a weaker

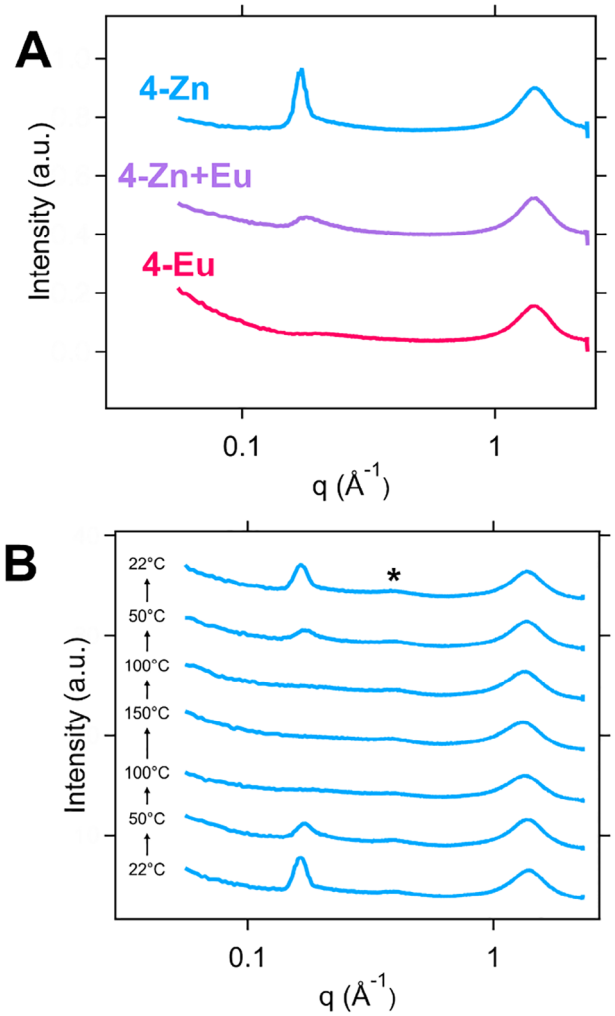

Figure 3. (A) Room temperature wide-angle x-ray scattering spectra of **4-Zn**, **4-Zn+Eu**, and **4-Eu**; (B) Temperature-dependent wide angle x-ray scattering spectra of **4-Zn** heated across a range of temperature from 22°C to 150°C and back to 22°C. The feature at q = 0.38 Å^{-1} (d = 16.5 Å) indicated by an asterisk corresponds to the polyimide tape used to seal the samples.

intensity signal at q = 0.16 Å^{-1} is present (Figure 3A) at room temperature, which suggests that the increase in Eu(III) content diminishes local LC ordering. This is hypothesized to be a consequence of an increase in the number of potential branching points resulting from the formation of the Eu:Bip$_3$ complex. As with the other samples at elevated temperatures, this weak peak disappears (Figure S15).

To probe the temperature-dependent short-time scale mechanical properties of the MSLCP materials, small angle oscillatory shear (SAOS) rheology experiments were performed (Figure 4A). The measured storage moduli (G') for all samples display three characteristic transitions. The first transition at approximately 12°C for **4-Zn**, **4-Zn+Eu**, and **4-Eu** corresponds to T_g and appears as a stepwise drop in the G' and a peak in the tan(δ) suggesting that variations in the metal content and subsequent supramolecular architecture have little effect on the T_g for these materials. The second transition is assigned to the T_C and manifests as a local minimum in the G' and a step in the

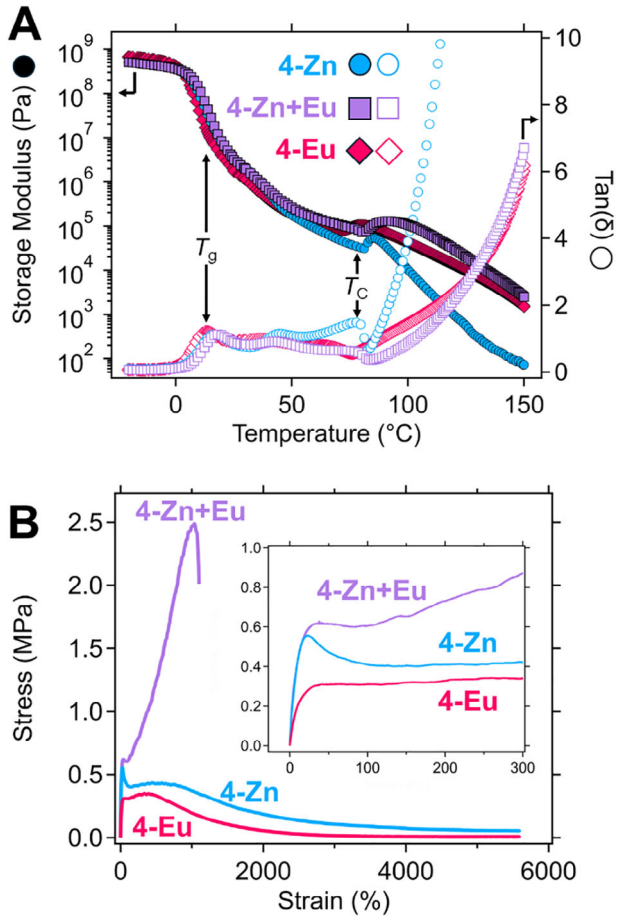

Figure 4. (A) Shear rheology dynamic temperature ramps of storage modulus (solid shapes) and tan(δ) (empty shapes) for MSLCPs; (B) Stress-strain profiles for MSLCPs.

tan(δ) appearing at 81°C, 80°C, and 70°C for **4-Zn**, **4-Zn+Eu**, and **4-Eu** respectively. These data are consistent with the T_C trend observed in the DSC when replacing the Zn(II) ions with Eu(III) ions in these MSLCP materials. The third transition manifests as a downward slope in G' and a sharp increase in tan(δ) indicating the onset of bulk flow in the materials. In all three MSLCPs, this transition occurs immediately after the T_C suggesting that the LC interactions play a large part in the robustness of the materials as the films lose cohesion once the material enters the isotropic state. In addition, there does not appear to be an observable change in the rheology indicative of the T_{UT} which further suggests that the LC character is responsible for the majority of the mechanical properties. The MSLCPs were also tested for their nonlinear mechanical properties using tensile testing at ambient conditions. Rectangular bars of **4-Zn**, **4-Zn+Eu**, and **4-Eu** were elongated at a constant strain rate (5 mm min^{-1}) until failure or reaching the maximum testing length of the instrument (Figure 4B). **4-Eu** displayed a curve shape representative of a soft and extensible material with a relatively low yield stress (σ_y) of 0.3 MPa and a maximum measured strain of around 5500% while the stress gradually decayed to zero stress across the strain range. **4-Zn** displayed a curve shape more consistent with a yielding plastic, with a higher σ_y of 0.6 MPa and yield strain (ε_y) of 40% while decaying out to a stress of 0.1 MPa and a maximum measured strain of >5500%. It is important to note that none of the tested samples of **4-Zn** or **4-Eu** could be strained to failure with the specified sample geometry and testing apparatus. Interestingly, the **4-Zn+Eu** film exhibited a very different behavior that deviates significantly from the stress decays and high extensions observed in the **4-Zn** and **4-Eu** samples. These films exhibited a strain-hardening behavior and a much larger maximum stress before failing around 1000%. One hypothesis for this behavior is that the mixture of both a strong and a weak binder in the Zn:Bip and Eu:Bip complexes enables rearrangement while maintaining structure, which allows the network to reorganize while strengthening.

Spent tensile samples were then collected to characterize the alignment of the resulting materials post-straining. This was probed using polarised optical microscopy (POM) imaging and wide angle X-ray scattering (WAXS) experiments. For POM measurements, samples were cut from the center of the spent tensile bar and placed on glass slides after being allowed to relax at room temperature for 5 min. The samples were then imaged at both 0° and 45° relative to the direction of the polarizer to visually determine the coherence of the strain-induced alignment imparted to the materials. All samples exhibited high levels of alignment (Figure 5A) as evidenced by the stark contrast in the transmitted brightness between the 0° and 45° images for each sample tested. To better quantify this behavior, WAXS experiments (Figure 5B) were performed on the previously strained MSLCP materials to determine the amount of alignment that can be achieved. As expected, the strained samples of **4-Zn**, **4-Zn+Eu**, and **4-Eu** exhibit an anisotropic 2D WAXS pattern (Figure 5B) with regions of intensity along the horizontal axis corresponding to the alignment of mesogens in the direction of applied strain along the vertical axis. By converting these images into plots of scattering intensity versus azimuthal angle (Figure 5C), fitting them using the Kratky method[77], and calculating the Hermans order parameter (S)[78] for the aligned materials, it is possible to compare the overall alignment in the MSLCP samples. The samples of **4-Zn**, **4-Zn+Eu**, and **4-Eu** possessed order parameter values of $S = 0.39$, $S = 0.34$, and $S = 0.30$ respectively. This decrease in S value with an increasing amount of Eu(III) ions may be related to the weaker binding of the Eu(III) and/or an increase in the potential branching points at the Eu(III) metal center that results in less strain-induced mesogenic alignment.

As both LCPs[79] and supramolecular polymers[80,81] have been studied as adhesive materials, the room temperature stress relaxation and pressure-sensitive probe tack behavior of the MSLCPs were also evaluated. Room temperature (22°C) shear stress relaxation experiments (3% strain, 1 h) (Figure 6A) were performed to determine how the different metal ions impact the dissipative nature of the MSLCPs. Akin to what is observed in recent studies on LCE adhesives[20,79,82], all the MSLCP materials rapidly dissipate stress, with **4-Zn**, **4-Zn+Eu**, and **4-Eu** dropping to 14%, 14%, and 7% of their initial applied stress value over the course of 60 s. As the majority of the applied stress (> 90%) had dissipated in the first 60 s, this time point was used to perform probe tack tests (Figure 6B) where a stainless-steel fixture was

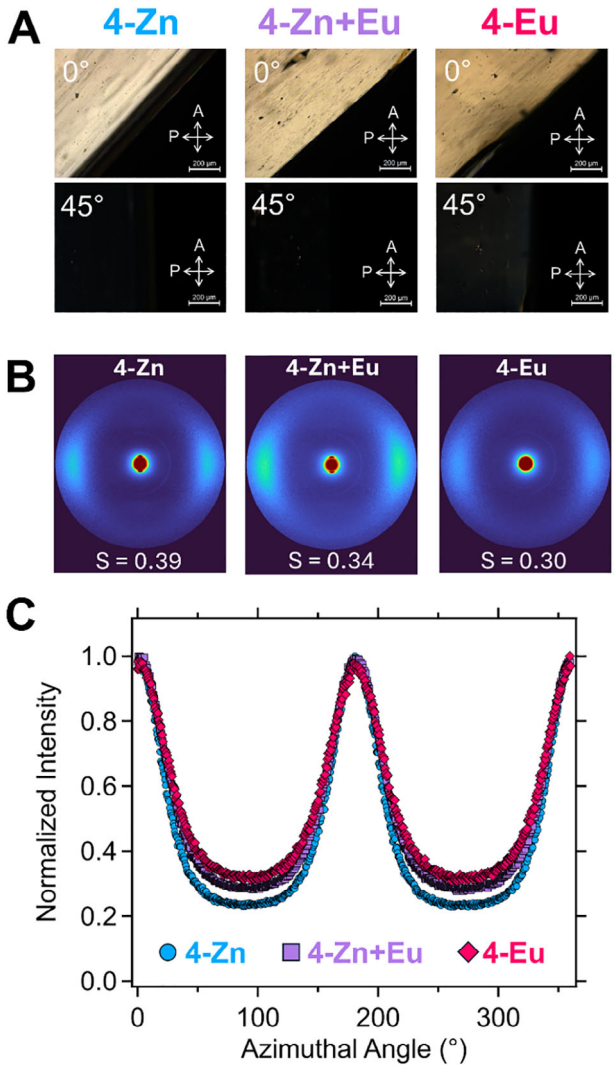

Figure 5. (A) Polarized optical microscopy images at 0° and 45° (B) 2D WAXS images of strained MSLCPs; (C) Plots of normalized intensity as a function of azimuthal angle for strained MSLCPs.

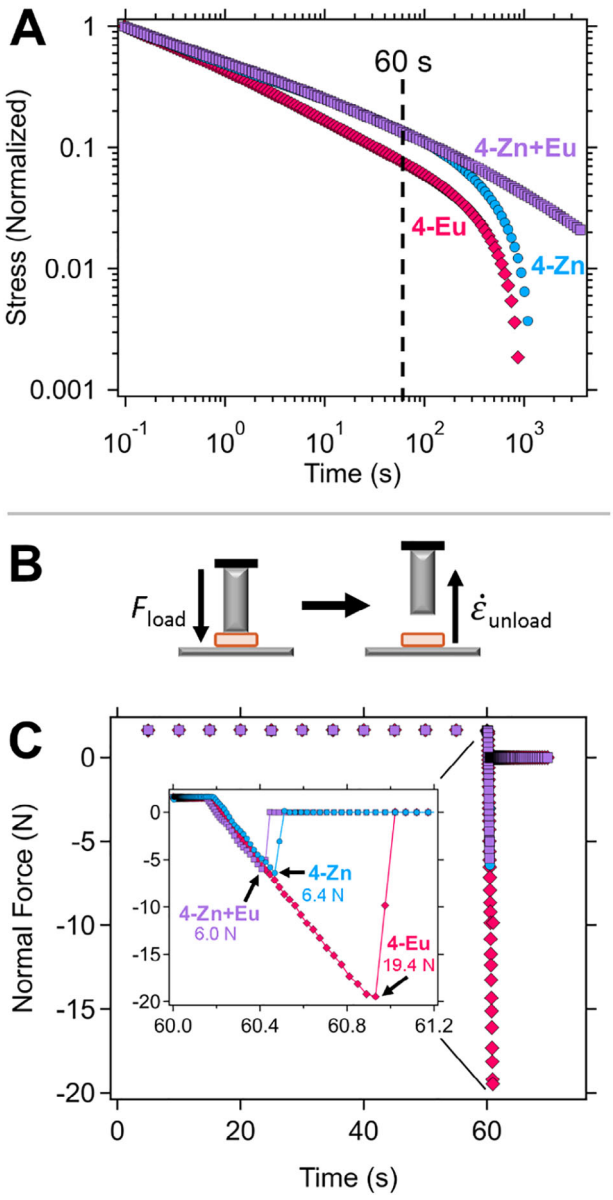

Figure 6. (A) Room temperature stress relaxation curves for MSLCPs; (B) General schematic for the probe tack test; (C) A representative force curve as a function of time for a single probe tack test; (inset) zoomed in view of debonding event.

pressed into a disk of MSLCP at a constant force and time (1 N, 60 s) after which the probe was retracted at a constant rate (0.1 mm s^{-1}), and the pull-off force required to break contact with the sample was measured (Figure 6C). For **4-Zn**, **4-Zn+Eu**, and **4-Eu**, the sample required pull-off forces of 6.4, 6.0, and 19.4 N respectively which are comparable to other LCP PSAs that have been studied.[20,79,83] The probe tack results also trend with the stress relaxation data in that at 60 s, **4-Zn** and **4-Zn+Eu** both have similar stress dissipations and pull-off forces while **4-Eu** has a higher stress dissipation correlating to higher pressure-sensitive adhesive response.

Hot melt adhesive (HMA) testing was then performed to demonstrate the utility of the bulk flow behavior exhibited by the MSLCP materials. As previously demonstrated in the temperature-dependent rheology data, the onset of bulk flow for all MSLCP materials occurs upon reaching T_C. However, the highest thermal transition (T_{UT}) based on the DSC thermograms does not occur until 130°C, so in pursuit of a robust adhesive joint, 3 mm diameter disk-shaped samples of each of the MSLCPs were placed between two aluminum I-bar fixtures, fixed in place with quarter inch binder clips, heated to 130°C for 2 min, and allowed to cool to room temperature. The adhesive strength of these fixtures was then measured via uniaxial tensile testing where the adhesive strength was taken as the maximum stress achieved prior to failure (Figure 7A). For **4-Zn**, **4-Zn+Eu**, and **4-Eu** the materials demonstrated respectable adhesive strengths of 4.5 ± 0.6 MPa, 8.5 ± 1.3 MPa, and 7.6 ± 1.1 MPa respectively. As evidenced by the representative images displayed in Figures 7B–D, all these materials present regions of material on each of the I-bars used to form the adhesive joint consistent with cohesive failure. To further contextualize the utility of this enhanced HMA strength, a 5 mm disk (thickness = 0.43 mm, mass = ~10 mg)

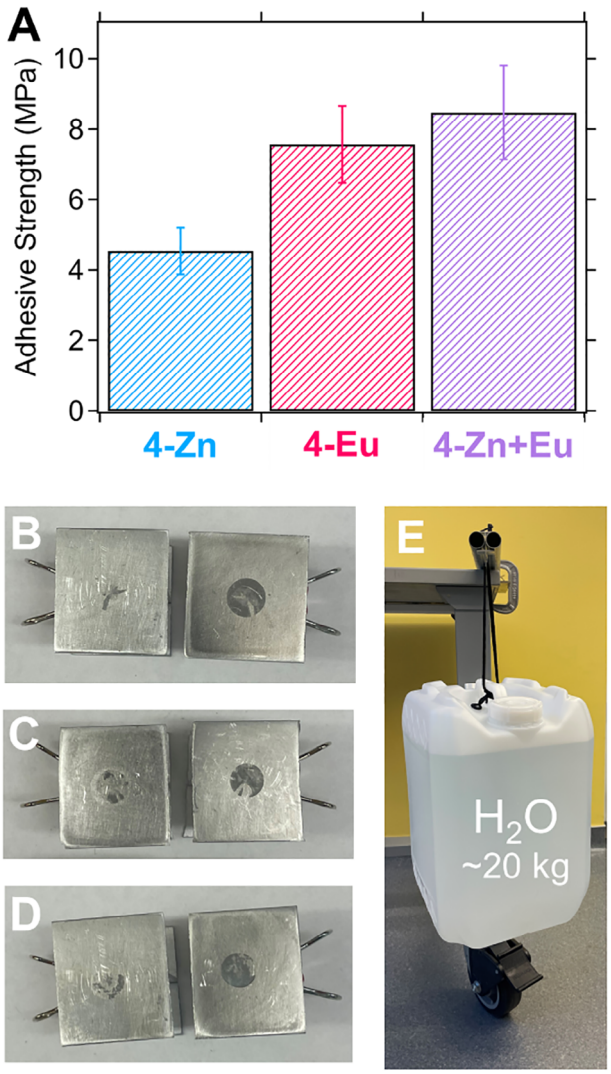

Figure 7. (A) Adhesive strength comparison of **4-Zn**, **4-Eu**, and **4-Zn+Eu**; (B) Representative sample of **4-Zn** after testing to failure; (C) Representative sample of 4-Zn+Eu after testing to failure; (D) Representative sample of **4-Eu** after testing to failure; (E) Demonstration of a sample of **4-Zn+Eu** supporting the weight of a 20 kg carboy filled with water

of **4-Zn+Eu** was used to form an adhesive joint between two aluminum I-bars which was capable of fully supporting a carboy filled with ~20 kg of water (Figure 7C).

3. Conclusion

In this work, metal-ligand interactions were utilized to develop a series of phase-separated MSLCPs whose thermomechanical, viscoelastic, and morphological properties were tailored through the selection of the linking metal ion. The choice of metal ions impacted the dynamic connectivity of the polymer architecture and subsequently altered the materials' characteristic thermal transitions, namely the T_g, T_C, and T_{UT} as measured by DSC and SAOS rheology techniques. In addition, the nonlinear mechanical properties studied via tensile testing of these materials were found to depend drastically on the identity of the incorporated metal ion with a strain hardening phenomenon only observed in the system with a mixture of metals (**4-Zn+Eu**). As the materials studied herein displayed high-stress dissipation and terminal flow behavior, these materials were studied for their adhesive character in both PSA and HMA contexts. The MSLCPs displayed robust PSA adhesive behavior that could be tailored through the nature of the metallosupramolecular bond, while HMA behavior trended with the modulus of the bulk material. These results demonstrate that tunable phase-separated MSLCPs are capable of forming tough (re)processable materials with potential applications as multi-level adhesives.

Supporting Information

Additional details regarding synthesis and characterization of materials including UV-Vis spectra, ^{1}H-NMR spectra, TGA curves, DSC curves, optical images, AFM images, and TWAXS spectra are located in the Supporting Information. The authors have also cited additional references within the Supporting Information.[84–88]

Acknowledgments

This work was primarily supported by the University of Chicago Materials Research Science and Engineering Center (IRG1) which is funded by the National Science Foundation under award number DMR-2011854. Additional support came from the National Science Foundation under award number CHE-2304633. N.R.B. was supported by a NASA Space Technology Graduate Research Opportunity at the NASA Glenn Research Center. Parts of this work were carried out at the Soft Matter Characterization Facility and the Materials Research Science and Engineering Center (MRSEC NSF DMR-2011854) at the University of Chicago. The authors would also like to thank Dr. Sarah Brown for her helpful advice during the revision of this manuscript.

Conflicts of Interest

The authors declare no conflicts of interest.

Data Availability Statement

The data that support the findings of this study are available from the corresponding author upon reasonable request.

Keywords: adhesive · liquid crystal polymer · metallosupramolecular interaction · noncovalent interactions · phase separation

[1] T. Kato, J. Uchida, T. Ichikawa, B. Soberats, *Polym. J.* **2018**, *50*, 149.
[2] X. Lyu, A. Xiao, D. Shi, Y. Li, Z. Shen, E. Q. Chen, S. Zheng, X. H. Fan, Q. F. Zhou, *Polymer* **2020**, *202*, 122740.
[3] P. G. De Gennes, *C. R. Acad. Sci. B* **1975**, *281*, 101.

[4] H. Finkelmann, H.-J. Kock, G. Rehage, *Die Makromol. Chemie, Rapid Commun.* **1981**, *2*, 317.
[5] M. Warner, E. M. Terentjev, *International Series of Monographs on Physics: Liquid Crystal Elastomers*, Oxford University Press, Oxford, **2007**.
[6] J. Gao, Y. He, X. Cong, H. Yi, J. Guo, *ACS Appl. Mater. Interfaces* **2022**, *14*, 53348.
[7] L. D. C. de Castro, T. A. P. Engels, O. N. Oliveira, A. P. H. J. Schenning, *ACS Appl. Mater. Interfaces* **2024**, *16*, 14144.
[8] K. R. Schlafmann, M. S. Alahmed, H. M. Pearl, T. J. White, *ACS Appl. Mater. Interfaces.* **2024**, *16*, 23780.
[9] K. A. Burke, P. T. Mather, *J. Mater. Chem.* **2010**, *20*, 3449.
[10] B. Jin, J. Liu, Y. Shi, G. Chen, Q. Zhao, S. Yang, *Adv. Mater.* **2022**, *34*, 2107855.
[11] W. Feng, Q. He, L. Zhang, *Adv. Mater.* **2024**, 2312313.
[12] C. Luo, C. Chung, N. A. Traugutt, C. M. Yakacki, K. N. Long, K. Yu, *ACS Appl. Mater. Interfaces.* **2021**, *13*, 12698.
[13] D. Mistry, N. A. Traugutt, B. Sanborn, R. H. Volpe, L. S. Chatham, R. Zhou, B. Song, K. Yu, K. N. Long, C. M. Yakacki, *Nat. Commun.* **2021**, *12*, 6677.
[14] H. Guo, A. Terentjev, M. O. Saed, E. M. Terentjev, *Sci. Rep.* **2023**, *13*, 10035.
[15] Q. He, Z. Wang, Y. Wang, A. Minori, M. T. Tolley, S. Cai, *Sci. Adv.* **2019**, *5*, eaax574.
[16] Y. Yao, E. He, H. Xu, Y. Liu, Z. Yang, Y. Wei, Y. Ji, *Nat. Commun.* **2023**, *14*, 3518.
[17] R. H. Volpe, D. Mistry, V. V. Patel, R. R. Patel, C. M. Yakacki, *Adv. Healthcare Mater.* **2020**, *9*, 1901136.
[18] S. Tasmim, Z. Yousuf, F. S. Rahman, E. Seelig, A. J. Clevenger, S. N. VandenHeuvel, C. P. Ambulo, S. Raghavan, P. E. Zimmern, M. I. Romero-Ortega, T. H. Ware, *Biomaterials.* **2023**, *292*, 121912.
[19] P. A. Pranda, A. Hedegaard, H. Kim, J. Clapper, E. Nelson, L. Hines, R. C. Hayward, T. J. White, *ACS Appl. Mater. Interfaces.* **2024**, *16*, 6394.
[20] H. Gou, S. Hou, M. O. Saed, *Adv. Mater. Interfaces.* **2024**, *11*, 2400488.
[21] Y. Wu, B. D. Clarke, K. M. Liechti, Z. A. Page, *Chem. Mater.* **2024**, *36*, 8066.
[22] S. J. Rowan, S. J. Cantrill, G. R. L. Cousins, J. K. M. Sanders, J. F. Stoddart, *Angew. Chemie–Int. Ed.* **2002**, *41*, 898.
[23] R. J. Wojtecki, M. A. Meador, S. J. Rowan, *Nat. Mater.* **2011**, *10*, 14.
[24] N. Zheng, Y. Xu, Q. Zhao, T. Xie, *Chem. Rev.* **2021**, *121*, 1716.
[25] C. Valenzuela, Y. Chen, L. Wang, W. Feng, *Chem.- Eur. J.* **2022**, *28*, e202201957.
[26] B. Jin, S. Yang, *Adv. Funct. Mater.* **2023**, *33*, 2304769.
[27] R. Lan, X. Hu, J. Chen, X. Zeng, X. Chen, T. Du, X. Song, H. Yang, *Responsive Mater.* **2024**, *2*, e20230030.
[28] Z. Pei, Y. Yang, Q. Chen, E. M. Terentjev, Y. Wei, Y. Ji, *Nat. Mater.* **2014**, *13*, 36.
[29] Z. Wang, H. Tian, Q. He, S. Cai, *ACS Appl. Mater. Interfaces* **2017**, *9*, 33119.
[30] J. Lee, J. Bae, J. H. Hwang, M. Choi, Y. S. Kim, S. Park, J. Na, D. Kim, S. Ahn, *Adv. Funct. Mater.* **2022**, *32*, 2110360.
[31] C. A. Lindberg, E. Ghimire, C. Chen, S. Lee, N. D. Dolinski, J. M. Dennis, S. Wang, J. J. de Pablo, S. J. Rowan, *J. Polym. Sci.* **2024**, *62*, 907.
[32] Z. Lei, H. Chen, S. Huang, L. J. Wayment, Q. Xu, W. Zhang, *Chem. Rev.* **2024**, *124*, 7829.
[33] E. Ghimire, C. A. Lindberg, T. D. Jorgenson, C. Chen, J. J. de Pablo, N. D. Dolinski, S. J. Rowan, *Macromolecules* **2024**, *57*, 682.
[34] K. M. Herbert, P. T. Getty, N. D. Dolinski, J. E. Hertzog, D. de Jong, J. H. Lettow, J. Romulus, J. W. Onorato, E. M. Foster, S. J. Rowan, *Chem. Sci.* **2020**, *11*, 5028.
[35] M. H. P. de Heer Kloots, S. K. Schoustra, J. A. Dijksman, M. M. J. Smulders, *Soft Matter* **2023**, 2857.
[36] N. R. Boynton, J. M. Dennis, N. D. Dolinski, C. A. Lindberg, A. P. Kotula, G. L. Grocke, S. L. Vivod, J. L. Lenhart, S. N. Patel, S. J. Rowan, *Science* **2024**, *383*, 545.
[37] N. D. Dolinski, R. Tao, N. R. Boynton, A. P. Kotula, C. A. Lindberg, K. J. Petersen, A. M. Forster, S. J. Rowan, *ACS Macro Lett.* **2024**, *13*, 174.
[38] S. Sivakova, D. A. Bohnsack, M. E. Mackay, P. Suwanmala, S. J. Rowan, *J. Am. Chem. Soc.* **2005**, *127*, 18202.
[39] M. Burnworth, L. Tang, J. R. Kumpfer, A. J. Duncan, F. L. Beyer, G. L. Fiore, S. J. Rowan, C. Weder, *Nature* **2011**, *472*, 334.
[40] Y. Chen, A. M. Kushner, G. A. Williams, Z. Guan, *Nat. Chem.* **2012**, *4*, 467.
[41] R. J. Wojtecki, A. Nelson, *J. Polym. Sci. Part A Polym. Chem.* **2016**, *54*, 457.
[42] J.-M. Lehn, *Angew. Chem., Int. Ed.* **1990**, *29*, 1304.
[43] L. Brunsveld, B. J. B. Folmer, E. W. Meijer, R. P. Sijbesma, *Chem. Rev.* **2001**, *101*, 4071.
[44] T. F. A. De Greef, M. M. J. Smulders, M. Wolffs, A. P. H. J. Schenning, R. P. Sijbesma, E. W. Meijer, *Chem. Rev.* **2009**, *109*, 5687.
[45] T. Aida, E. W. Meijer, S. I. Stupp, *Science* **2012**, *335*, 813.
[46] K. M. Herbert, S. Schrettl, S. J. Rowan, C. Weder, *Macromolecules* **2017**, *50*, 8845.
[47] L. Hammer, N. J. Van Zee, R. Nicolaÿ, *Polymers* **2021**, *13*, 396.
[48] U. S. Schubert, C. Eschbaumer, *Angew. Chemie., Int. Ed.* **2002**, *41*, 2892.
[49] S. J. Rowan, J. B. Beck, *Faraday Discuss.* **2005**, *128*, 43.
[50] M. Burnworth, D. Knapton, S. J. Rowan, C. Weder, *J. Inorg. Organomet. Polym. Mater.* **2007**, *17*, 91.
[51] G. R. Whittell, M. D. Hager, U. S. Schubert, I. Manners, *Nat. Mater.* **2011**, *10*, 176.
[52] A. Winter, U. S. Schubert, *Chem. Soc. Rev.* **2016**, *45*, 5311.
[53] S. Ghiassinejad, K. Mortensen, M. Rostamitabar, J. Malineni, C. A. Fustin, E. Van Ruymbeke, *Macromolecules* **2021**, *54*, 6400.
[54] S. Coulibaly, C. Tchambaga Etienne, A. Koné, A. F. Kouassi, C. Siomenan, *Adv. Polym. Technol.* **2024**, *2024*, 1782876.
[55] F. Biedermann, H. J. Schneider, *Chem. Rev.* **2016**, *116*, 5216.
[56] Y. L. Rao, A. Chortos, R. Pfattner, F. Lissel, Y. C. Chiu, V. Feig, J. Xu, T. Kurosawa, X. Gu, C. Wang, M. He, J. W. Chung, Z. Bao, *J. Am. Chem. Soc.* **2016**, *138*, 6020.
[57] Y. L. Rao, V. Feig, X. Gu, G. J. Nathan Wang, Z. Bao, *J. Polym. Sci. Part A Polym. Chem.* **2017**, *55*, 3110.
[58] L. N. Neumann, I. Gunkel, A. Barron, E. Oveisi, A. Petzold, T. Thurn-Albrecht, S. Schrettl, C. Weder, *Macromolecules* **2020**, *53*, 5068.
[59] Y. Li, C. Pyromali, F. Zhuge, C.-A. Fustin, J.-F. Gohy, D. Vlassopoulos, E. van Ruymbeke, *J. Rheol.* **2022**, *66*, 1203.
[60] R. D. Mukhopadhyay, A. Ajayaghosh, *Chem. Soc. Rev.* **2023**, *52*, 8635.
[61] P. N. Johnson, Y. Yao, X. Huang, I. Kevlishvili, S. Schrettl, C. Weder, H. J. Kulik, S. L. Craig, *Polymer* **2023**, *285*, 126337.
[62] H. Park, T. Kang, H. Kim, J.-C. Kim, Z. Bao, J. Kang, *Nat. Commun.* **2023**, *14*, 5026.
[63] B. T. Michal, B. M. McKenzie, S. E. Felder, S. J. Rowan, *Macromolecules* **2015**, *48*, 3239.
[64] C. Zhang, G. Fei, X. Lu, H. Xia, Y. Zhao, *Adv. Mater.* **2024**, *36*, 2307210.
[65] S. J. A. Houben, S. J. D. Lugger, R. J. H. Van Raak, A. P. H. J. Schenning, *ACS Appl. Polym. Mater.* **2022**, *4*, 1298.
[66] R. Liang, H. Yu, L. Wang, D. Shen, *Adv. Funct. Mater.* **2023**, *33*, 2211914.
[67] J. B. Beck, S. J. Rowan, *J. Am. Chem. Soc.* **2003**, *125*, 13922.
[68] J. B. Beck, J. M. Ineman, S. J. Rowan, **2005**, *38*, 5060.
[69] J. R. Kumpfer, J. J. Wie, J. P. Swanson, F. L. Beyer, M. E. MacKay, S. J. Rowan, *Macromolecules* **2012**, *45*, 473.
[70] S. Coulibaly, C. Heinzmann, F. L. Beyer, S. Balog, C. Weder, G. L. Fiore, *Macromolecules* **2014**, *47*, 8487.
[71] L. N. Neumann, E. Oveisi, A. Petzold, R. W. Style, T. Thurn-Albrecht, C. Weder, S. Schrettl, *Sci. Adv.* **2021**, *7*, eabe4154.
[72] C. Piguet, J. C. G. Bünzli, G. Bernardinelli, G. Hopfgartner, A. F. Williams, *J. Alloys Compd.* **1995**, *225*, 324.
[73] M. Enamullah, W. Linert, *J. Coord. Chem.* **1996**, *40*, 193.
[74] H. J. Hong, S. Y. Park, *J. Ind. Eng. Chem.* **2022**, *110*, 424.
[75] J. Sautaux, L. M. De Espinosa, S. Balog, C. Weder, *Macromolecules* **2018**, *51*, 5867.
[76] F. Marx, M. Beccard, A. Ianiro, A. Dodero, L. N. Neumann, G. Stoclet, C. Weder, S. Schrettl, *Macromolecules* **2023**, *56*, 7320.
[77] M. T. Sims, L. C. Abbott, R. M. Richardson, J. W. Goodby, J. N. Moore, *Liq. Cryst.* **2019**, *46*, 11.
[78] J. J. Hermans, P. H. Hermans, D. Vermaas, A. Weidinger, *Recl. Trav. Chim. Pays-Bas* **1946**, *65*, 427.
[79] H. Guo, M. O. Saed, E. M. Terentjev, *Macromolecules* **2023**, *56*, 6247.
[80] C. Heinzmann, C. Weder, L. M. De Espinosa, *Chem. Soc. Rev.* **2016**, *45*, 342.
[81] P. Sun, B. Qin, J. Xu, X. Zhang, *Macromol. Chem. Phys.* **2023**, *224*, 2200332.
[82] H. J. Farre-Kaga, M. O. Saed, E. M. Terentjev, *Adv. Funct. Mater.* **2022**, *32*, 2110190. https://doi.org/10.1002/adfm.202110190.

[83] T. Ohzono, M. O. Saed, E. M. Terentjev, *Adv. Mater.* **2019**, *31*, 1902642.
[84] P. Froidevaux, J. M. Harrowfield, A. N. Sobolev, *Inorg. Chem.* **2000**, *39*, 4678.
[85] C. J. Rao, K. A. Venkatesan, K. Nagarajan, T. G. Srinivasan, P. R. Vasudeva Rao, *Electrochim. Acta.* **2009**, *54*, 4718.
[86] M. C. Wilkinson, M. Higson, *Org. Process Res. Dev.* **2017**, *21*, 75.
[87] Y. Barre, M. Simon, R. Neige, R. Duval, *Ureido or Carbamate Derivatives of Crown Ethers and of Silicon usable for Preparing Supports Intended for the Separation by Chromatography of Metal Cations and of Organic Molecules Comprising Amine Functional Groups*, **2007**, US7230123B2.
[88] S. V. Arehart, C. Pugh, *J. Am. Chem. Soc.* **1997**, *119*, 3027.

Manuscript received: December 19, 2024
Revised manuscript received: March 16, 2025
Version of record online: April 8, 2025